Astron. Astrophys. 334, 1068–1084 (1998)

ASTRONOMY AND ASTROPHYSICS

Interstellar modulation of the flux density and arrival time of pulses from pulsar B 1937+214

J.-F. Lestrade[1], **B.J. Rickett**[2], **and I. Cognard**[3]

[1] Observatoire de Paris, Meudon, F-92195 Meudon, France
[2] Department of Electrical and Computer Engineering, University of California at San Diego, CA 92093-0407, USA
[3] LPCE-CNRS, 3A, Av. de la Recherche Scientifique, F-45071 Orléans, France

Received 1 September 1997 / Accepted 10 February 1998

Abstract. Observations of the millisecond pulsar B1937+214 made at Nançay over 6 years show 30% rms flux variations over 13 ± 4 days due to Refractive Interstellar Scintillations. The arrival times (TOA) also show variations over a similar time scale 16 ± 10 days with an rms amplitude of about 0.3μsecs. These "rapid" TOA variations are anti-correlated ($\sim -40\%$) with the flux and so are also caused by propagation through the ionized interstellar medium. The correlation is such that weak pulses tend to arrive late. While TOA modulations due to changing geometric delay should be positively correlated with flux, those due to small scale variations in the dispersive delay should be negatively correlated with the flux and so are presumed to be responsible in our observations. The level and time scales are shown to be consistent with expectations based on the Kolmogorov model of the interstellar density spectrum. However, in the data there is a sequence of about 5 discrete events, in which the flux remains low over 10-30 days and the TOA is on average late but also shows rapid variations. Assuming that these are indeed discrete events, we interpret them as due to isolated regions of enhanced plasma density crossing the line of sight. Such "Extreme Scattering Events" make a major contribution to the TOA variations and their anti-correlations with the observed flux. They are seen against a background of the normal refractive scintillation. A model is proposed in which discrete sheets of plasma cross the line of sight and cause a "de-focussing" event when aligned parallel to the line of sight. The statistics of the events imply a surprisingly large space density of the sheets; an alternative is that by chance we view PSR B1937+214 tangentially through a supernova shell which is fragmented and so causes multiple events.

Key words: pulsars: general – pulsars: individual: PSR B1937+214 – scattering – ISM: general

1. Introduction

The millisecond pulsar B1937+214 has been very closely studied in the 15 years since its discovery (Backer et al. 1982). The extraordinary precision with which its pulse arrival time can be measured and its remarkable rotational stability (e.g. Kaspi et al. 1994 [KTR94] and Cognard et al. 1995 [C95]) have opened many new applications for pulsar timing measurements. In addition to studies of the dynamics of rotating neutron stars, there are prospects of developing an astronomical time reference as precise as the best on Earth and even detecting cosmic gravitational waves.

The influence of the ionised interstellar medium on the pulse arrival time is centrally important. In order to reveal the emitted pulse shape, the smearing of the pulse by the dispersive sweep across the receiver bandpass has to be compensated for and several techniques have now been successfully developed. The need to measure the arrival time at two or more radio frequencies to monitor and correct for changes in the interstellar dispersion delay is now well documented (Cordes et al. 1990 and KTR94). These measurements have also yielded new estimates of the large scale structure of the interstellar plasma density from a structure function analysis of the changing dispersion measure. Interstellar scintillation acts to perturb the pulse arrival time when the observations cover only a few independent samples of the diffractive scintillation in frequency and time (Cordes et al. 1990). Wide bandwidths and long integration times are used in timing observations to reduce such diffractive effects. Refractive effects also modulate the flux on typical time scales of days to months. There should be associated small modulations of the arrival time due to the longer path of refracted waves. There are few observed examples of such refractive arrival time modulations, though the theory of how the interstellar plasma can modulate the pulse arrival times has been discussed by several authors (e.g. Blandford & Narayan, 1985 [BN]; Cordes, Pidwerbetsky & Lovelace, 1986 [CPL]; Romani, Narayan & Blandford, 1986 [RNB]; Foster & Cordes, 1990).

The two most complete series of arrival time observations for PSR B1937+214 are those of KTR94 at Arecibo and C95 at Nançay. After correcting for the pulsar position and spindown model ($\dot{P}$) and the changing interstellar dispersion delay, these observers report a timing residual, which has a quasi sinusoidal variation of a few microseconds over about six years. This slow variation is thought to be an intrinsic rotational instability of the pulsar, and when it is removed, the residual arrival times appear to vary randomly. At 1.4 GHz these residual TOA variations have an rms of about 0.4 μsec in both data sets, implying that

they are not limited by signal to noise ratio, which is considerably better at Arecibo. Further the Arecibo observations at 2.3 GHz have a lower rms of 0.2 μsec, which suggests an inverse frequency dependence, as might be caused by a plasma propagation process. The purpose of this paper is to report such an interstellar propagation contribution to the timing residuals in the Nançay data and their relation to variations in the pulse flux.

In Cognard et al. (1993) [C93] we identified an "extreme scattering event" from the simultaneous perturbations of the flux and arrival times, made possible by the relatively frequent sampling of the observations. Several more such events have since been found in the data, as reported by Cognard & Lestrade (1996). We earlier found (Lestrade, Cognard & Biraud, 1995; hereafter LCB) an anti-correlation between the timing residual and the pulse flux. The purpose of this paper is to reanalyze this anti-correlation and the associated theory and also to examine the influence of the extreme scattering events. In Sect. 2 we describe the observations, in Sect. 3 we give the correlation analysis, in Sect. 4 we discuss the interpretation as Interstellar Scintillation, in Sect. 5 we give a discussion of the structures responsible in the interstellar medium, and in Sect. 6 we summarize our conclusions.

2. Observations and ANTIOPE analysis

Timing observations of PSR B1937+214 are conducted at the decimetric radio telescope located near Nançay (France). The collecting area of the telescope is 7000 m^2 (equivalent to a 93 meter dish) and the system temperature is typically $\sim$ 45 K. The integration time with this transit telescope is 70 minutes at the declination of PSR B1937+214. The pulsar signal is dedispersed by using a swept frequency oscillator (at 80 MHz) in the receiver IF chain. This oscillator is a slaved Voltage Control Oscillator (VCO) driven by a saw-tooth wave form, synthesized in steps of 100 ns to produce a parabolic frequency sweep precisely tracking the interstellar dispersion law. The frequency range swept by this oscillator is 7.55 MHz, which is the dispersion bandwidth at 1410 MHz corresponding to the 1.56 msec period of PSR B1937+214 with DM = 71.04 cm^{-3}pc. The pulse spectra are produced by the station digital autocorrelator with a frequency resolution of 6.25 kHz. The "Frequency Of Arrival" is measured by cross-correlation between the daily pulse spectrum and the pulse spectrum template, and then converted into the corresponding Time of Arrival (TOA). The station UT time scale is provided by a Rhode and Schwarz XSRM Rubidium Frequency standard and the offset relative to the international UTC time scale is measured daily at 14 UT via the Observatory of Paris by a special purpose receiver using TV signals. The accuracy of this daily monitoring is at the level of 40 nanosec as shown by various consistency cross-checks and several Global Positioning System (GPS) measurements conducted in parallel. The contribution from system noise to the errors in TOA estimates have not been fully evaluated. Our error estimates are typically 0.2 μsec; the clock step of 0.1 μsec triggering the VCO provides a hard lower limit to the measurement error and the observed residual of 0.4 μsec is an upper limit. Finally, the calibration of the pulse peak amplitude from autocorrelator units to Janskys is accurate to about 15 %.

Flux density variations caused by diffractive scintillation should be largely smoothed out by averaging the pulse signal over 70 minutes and over 7.5 MHZ at 1410 MHz. From measurements by Ryba (1991) the characteristic diffractive scintillation parameters for PSR B1937+214 are $\Delta\nu \approx 0.5$ MHz and $t_d \approx 7$ minutes, implying that in each daily average there are about 150 independent scintles; we estimate the residual modulation index due to diffractive scintillation to be 14% and the corresponding diffractive contribution to jitter in TOA to be very small (< 40 nsec).

The software ANTIOPE was developed at Meudon Observatory to adjust the relevant pulsar parameters (period, time-derivatives, position, proper motion, possibly trigonometric parallax, pulsar phase offsets, ...) to the TOA measurements by a least-squares-fitting procedure. In this software, a TOA is modelled as the propagation time of pulse n emitted by the pulsar at Solar System barycentric position $\boldsymbol{R}_n$ and coordinate-time T_n, and received by the radio telescope at barycentric position $\boldsymbol{r}_n$ and coordinate-time t_n:

$$T_n - t_n = \frac{|\boldsymbol{R}_n - \boldsymbol{r}_n|}{c} + \tau_R + \frac{k < DM >}{\nu^2} \quad (1)$$

τ_R is the Shapiro delay of General Relativity. The last term is the additional delay caused by the mean level of the total electron content of the ionized interstellar medium integrated along the line of sight and characterized by the mean Dispersion Measure $< DM >$.

Eq. (1) is expandable into a Taylor series of $\frac{1}{R_0}$ (pulsar distance R_0) and breaks into several geometrical terms as shown by Hellings (1986). Eq. (1) is complemented by the relativistic transformation between coordinate-time and measured time at the station. Finally, the rotation of the pulsar is modelled by its rotational phase :

$$\phi(T_n) = \phi_0 + \frac{1}{P_0}(T_n - T_0) - \frac{1}{2}\frac{\dot{P}_0}{{P_0}^2}(T_n - T_0)^2 - \frac{1}{6}\frac{\ddot{P}}{{P_0}^2}(T_n - T_0)^3 + ... \quad (2)$$

where ϕ_0, P_0, $\dot{P}_0$ and $\ddot{P}$ are the phase offset, the pulsar period and period derivatives at origin T_0, respectively.

In the TOA model of ANTIOPE, the barycentric position of the geocenter is read from the Jet Propulsion Laboratory DE202 (Standish 1982; Newhall, Standish & Williams, 1983) the terrestrial coordinates of Nançay are from the VLBI determination by Petit, Boucher & Lestrade (1989). Standard transformations for the precession and nutation are used to transform the terrestrial coordinates of Nançay to celestial coordinates and these transformations are complemented by the Earth Orientation Parameters (Pole motion (x,y) and UT1-UTC). The IAU conventions at epoch J2000 are implemented for all these transformations. The time scale of the measured TOA's is the conventional UTC time scale and the relativistic transformation between Terrestrial Time and Barycentric Time uses the analytical solution of

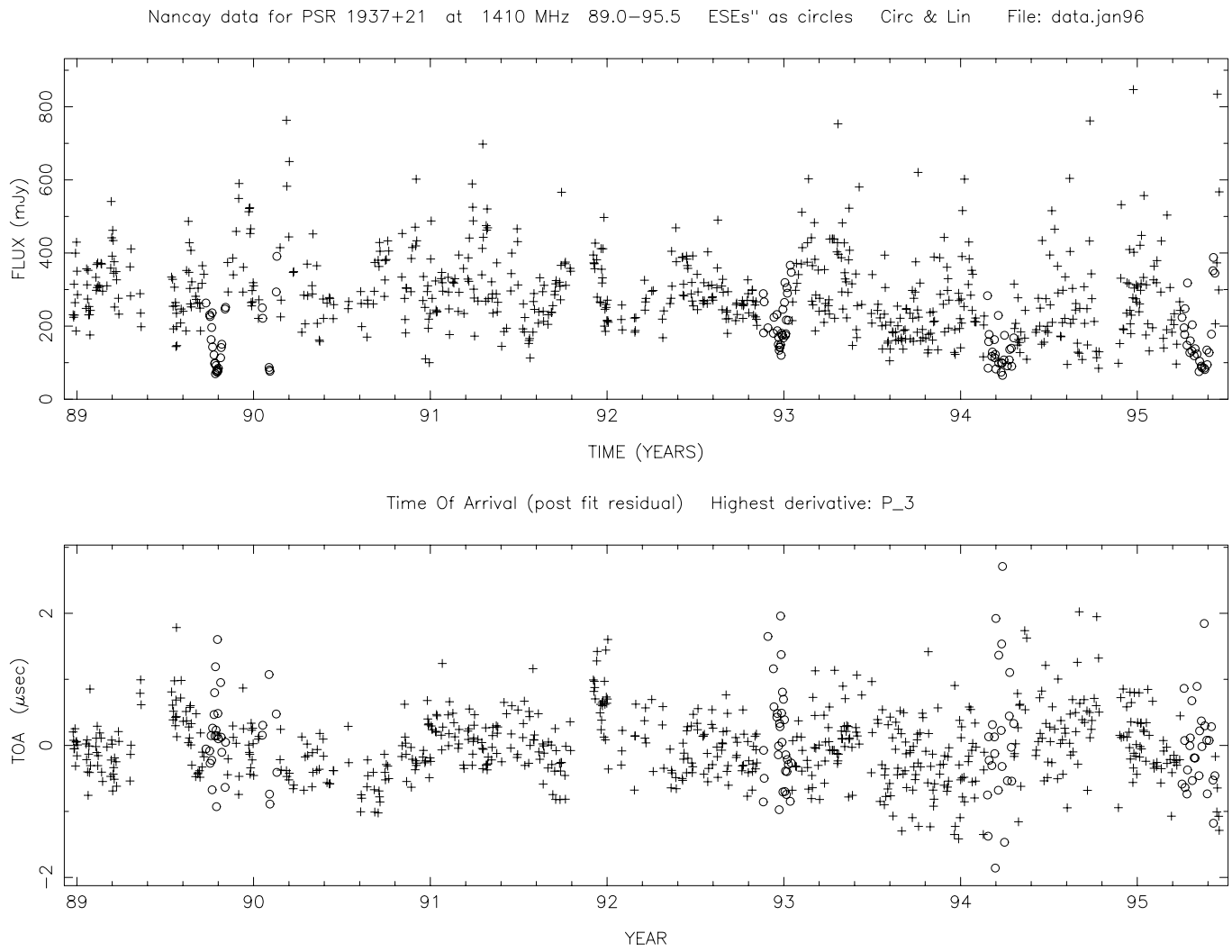

Fig. 1. PSR B1937+214 time series of the averaged pulse flux at 1.41 GHz and post-fit residual in the Time of Arrival (TOA) plotted as pluses, with periods identified as Extreme Scattering Events plotted as circles.

Fukushima (1988), where only the periodic terms are kept. In the following sections we analyze the post-fit timing residuals, to study the fluctuations caused by interstellar propagation effects not removed by the deterministic model of Eq. (1).

We have analysed two sets of data from the regular timing observations of PSR B1937+214 at Nançay started on December 22, 1988. TOA and flux densities were measured regularly 8 to 12 times per month at 1410 MHz in both senses of circular polarization until December 2, 1991. Subsequently, we observed the pulsar at 1.28, 1.41, 1.68 and 1.70 GHz but in the linear polarization mode. The combined data sets at 1.41 GHz are displayed in Fig. 1. Analysed separately, we find that the post-fit timing residual rms is significantly better for the circular polarization observations (rms = 0.39 μsec) than for the linear polarization observations (rms = 0.61 μsec). As we discuss below, the increased rms is due to the effects of varying ionospheric Faraday rotation. Consequently we have not included the TOA's from the linear polarization data in Fig. 2, which shows the time series of pulse flux at the three frequencies up to Dec 2, 1995, when circularly polarized observations were resumed.

Table 1. Parameters of PSR B1937+214 fitted to the TOA's measured in both senses of circular polarization at Nançay between December 22, 1988 and December 12, 1991 at 1410 MHz. The numbers in parenthesis are the formal uncertainties on the last digits.

Parameters	Fitted values
Period P_0 (s)	0.0015578064724486 16(3)
$\dot{P}_0$ (s/s)	$10.51209(2)\ 10^{-20}$
$\ddot{P}$ (s/s^{-2})	$-0.95(14)\ 10^{-31}$
α $(J2000)$	$19^h39^m38.558714(2)$
δ $(J2000)$	$21^\circ34'59.13746(3)$
μ_α (mas/yr)	$-0.26(2)$
μ_δ (mas/yr)	$-0.53(2)$
Time origin T_0 (JD)	2447900.0
Number TOA dates	321
Post-fit TOA rms	0.39 μsec

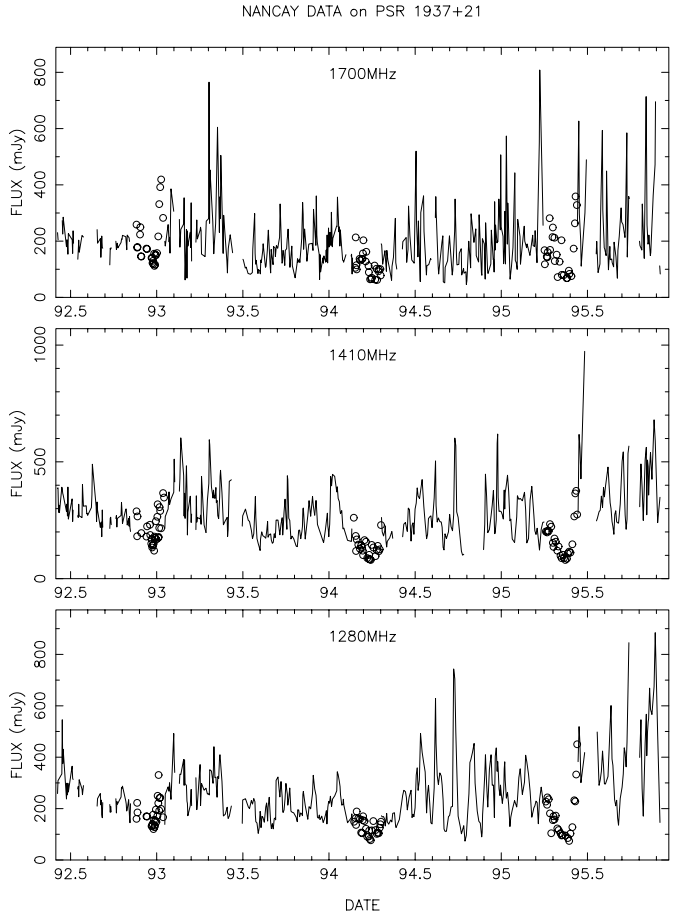

Fig. 2. Time series of averaged pulse flux from PSR B1937+214 at three radio frequencies (in linear polarization). Periods identified as Extreme Scattering Events are plotted as circles

PSR B1937+214 is 50 % linearly polarized with a P.A. swing of 90° at 1418 MHz (Thorsett 1991). This P.A. swing of the linear polarization components combines with the annual and secular variations of the Faraday Rotation of the ionosphere and interstellar medium (ISM) to modify the observed mean pulse profile shape. This effect will shift slightly the mean pulse profile peak from day to day, adding a variable delay to our timing measurements. One can show that the pulse profile peak shifts fractionally by $\frac{\alpha}{360^\circ}$ of the pulse width W, if α is the Faraday Rotation in degrees. Assuming a plausible variation of the ionospheric Rotation Measure of 1rd m^{-2}, the corresponding change in Faraday Rotation angle $\alpha \sim 2.5^\circ$ at 1400 MHz. Assuming the worst case for the intrinsic pulse profile, a square shape, and taking the P.A. swing of $\pm 90^\circ$ and pulse width $W = 35\mu$sec at 1410 MHz for PSR B1937+214, the expected systematic timing variation is $\frac{\alpha}{360^\circ} \times W \sim 0.3\mu$sec. Annual or long term variations of the Faraday Rotation from the ionosphere and ISM are absorbed by the pulsar parameter adjustment, resulting in slight biases of the pulsar position and period. The day-to-day variations increase the post-fit timing residual rms in our Nançay linear polarization observations, as noted above. This jitter is large enough to be seen as increased "noise" in the TOA's in Fig. 1 from 1992 onwards. Consequently, we put more weight on the circular polarization observations at 1410 MHz in the TOA-amplitude cross-correlation analysis developed below.

The adjustment of the 8 classical timing parameters $(\phi_0, P_0, \dot{P}_0, \ddot{P}, \alpha, \delta, \mu_\alpha, \mu_\delta)$ for the single pulsar B1937+214 has been made with ANTIOPE. The post-fit timing residual rms is 0.39 μsec in this adjustment, when $< DM >$ is kept constant (71.0037 cm^{-3} pc). This rms is not significantly different from the post-fit rms 0.40 μsec when the Arecibo 90-day smoothed DM variations (Ryba, 1991) are used. Table 1 shows the fitted values and, as expected, these pulsar parameters, especially the period, are slightly different from the values determined when the long-term variation of DM is modelled by the Arecibo DM series (*e.g.* Cognard *et al* 1993). However, this has no impact on the post-fit timing residuals used to study the short term variations of the TOA's in our present study.

In this adjustment, we have solved for $\ddot{P}$ to remove the "red noise" that is otherwise apparent in the residuals. We have also solved for higher time-derivatives of P (up to 7th order in tests), but this does not significantly improve the post-fit timing residual rms. A recent comparison between the fractional stabilities of the timing residuals of PSR B1937+214 and the angularly close millisecond pulsar PSR B1855+097 is interpreted as evidence that the red noise in PSR B1937+214 is an intrinsic rotation irregularity of the pulsar itself (KTR94).

As reported by Cognard et al (1993), an Extreme Scattering Event (ESE) was identified in October 1989, when the TOA residuals were systematically positive and the flux went through a pronounced minimum. In Fig. 1 we have used circles to flag this interval. We have also used circles to flag four other such intervals, which have also been identified as ESEs by Cognard & Lestrade (1996); however they are less well observed than the first event and their classification as ESEs is more tentative.

3. Correlation analysis

The random appearance of the variations in Figs. 1 and 2 suggest a correlation analysis, which we present in this section. The simplest explanation for the flux variations is Refractive Interstellar Scintillation (RISS), and indeed the 6-year data set at 1410 MHz provides an important long period for the study of RISS and the data in Fig. 2 provide a unique study of the frequency dependence of the phenomenon. Since RISS variations are stochastic, the correlation function (or structure function) provides a useful characterization. The data-sets are long enough that there is no clear advantage to the structure function and we present in Fig. 3 the auto-correlation function for the flux and for TOA residual and their cross-correlation for the data from Fig. 1.

Explicitly, the data are flux variations from their mean $\Delta\hat{F}_i$ and TOA residual $\Delta\hat{T}_i$ estimated at unevenly spaced times t_i. We form the covariance estimates in the usual way as:

$$\hat{C}_{xy}(\tau_l) = \frac{\Sigma_l^{i,j} \Delta x_i \Delta y_j}{\Sigma_l^{i,j} 1} \tag{3}$$

where x and y stand for either F or T. Thus we have two auto-covariance (ACV) estimates $\hat{C}_{FF}$, $\hat{C}_{TT}$ and a cross-covariance

$\hat{C}_{FT}$. The $\Sigma_l^{i,j}$ represents the summation over all data pairs with time difference $t_i - t_j$ lying within a window of width δp centered on $\tau_l = l\delta p$, where l is an integer and $\delta p = 1$day. In the top panel of Fig. 3 we plot the auto-correlation functions (ACFs), which are simply the normalized ACVs:

$$\hat{\rho}_{FF}(\tau_l) = \frac{\hat{C}_{FF}(\tau_l)}{\hat{C}_{FF}(0)} \tag{4}$$

and similarly for $\hat{\rho}_{FF}$. At zero lag $\hat{\rho}_{TT}$ equals unity and drops abruptly with increasing τ; this spike at zero lag is due to system noise and any rapidly varying pulsar process; also visible is a more slowly decreasing term that is our "signal" which decays over 10's of days. As discussed below we believe that this signal is caused by interstellar propagation.

3.1. Noise correction

Consider "noise" $n_{F,i}$, which includes any pulsar variations faster than one day, added to the slower flux deviation ΔF_i giving a measured flux deviation:

$$\Delta\hat{F}_i = \Delta F_i + n_{F,i} \tag{5}$$

and similarly the true TOA residual ΔT_i with its "noise" gives a measured TOA residual:

$$\Delta\hat{T}_i = \Delta T_i + n_{T,i} \tag{6}$$

Assuming that the two noise series are white and both independent of the signals F and T and independent of each other, the ensemble average of each C is simply the sum of the ACVs of the signal R_{FF} or R_{TT} and of the noise R_{nF} or R_{nT}. When the data sets are sufficiently long the ACV *estimates*, (denoted by a hat) are similarly the sum of signal and noise terms eg:

$$\hat{C}_{FF}(\tau_l) = \hat{R}_{FF}(\tau_l) + \hat{R}_{nF}(\tau_l) \tag{7}$$

Our goal is to estimate the ACV of the signals. Since the noise is white, $\hat{R}_{nF}(\tau_l)$ adds a spike at zero lag and, because it fluctuates about zero for all other time lags, it also contributes a rapidly fluctuating error term at other lags as evident in Fig. 3. Here the signals are the parts of the ACVs that remain correlated for some 10-20 days, and so to reduce these rapidly fluctuating errors we have smoothed the ACV estimates with a Gaussian function (5 day full width at 1/e), but excluding the zero lag point to eliminate the noise spike. We write these smoothed estimates as $\hat{Q}_{FF}$ and $\hat{Q}_{TT}$, which are plotted as solid lines versus positive lags for the flux and versus negative lags for the TOA, normalized in the same way as the data points (ie divided by $\hat{C}_{FF}(0)$ and $\hat{C}_{TT}(0)$). The lines show the correlation due to the signal more clearly than the points. We use $\hat{Q}_{FF}(0)$ and $\hat{Q}_{TT}(0)$ as our best estimate of the signal variances in ΔF and ΔT. Note that each also has a statistical error due to the finite length $T_{\rm obs}$ of the observing span.

Turning to the cross-covariance $\hat{R}_{FT}(\tau_l) = \hat{C}_{FT}(\tau_l)$, since the uncorrelated noises cause no bias, though they do contribute independent fluctuations versus time lag. In the lower panel of Fig. 3 are plotted the estimated cross-correlation functions, which are nomalized by the estimated signal variances:

$$\hat{\rho}_{FT}(\tau_l) = \frac{\hat{C}_{FT}(\tau_l)}{\sqrt{\hat{Q}_{FF}(0)\hat{Q}_{TT}(0)}} \tag{8}$$

The lower panel of Fig. 3 shows that at zero lag the flux and TOA residuals are anticorrelated, in the sense that weak pulses tend to be late. This result was already reported (LCB), and our goal here is to present it in more detail and to reexamine the interpretation. The anti-correlation is interesting because it flags part of the TOA fluctuations as due to interstellar propagation. We estimate the cross-correlation coefficient between F and T, by taking the zero lag value of $\hat{\rho}_{FT}(\tau_l)$ after first smoothing it by the same 5-day Gaussian function used in defining $\hat{Q}$. The result is an estimate of -0.36 $\pm$ 0.1 at zero lag, for the data of Fig. 1 (1989-1995); the filtering effect of the different fitted polynomials is discussed below in Sect. (4.2).

Fig. 3 shows the effects of both system noise and estimation error. System noise causes rapid fluctuations independent between each lag value and which are reduced in amplitude by the 5-day smoothing (solid line). In addition estimation error causes variations that are correlated over a range of time lags comparable to the refractive scintillation times exhibited in the auto-correlation functions; they come from the finite time span of the observations (6.5 years), which includes only a modest number of independent refactive scintillation times (10-20 days). These two terms determine the error in the zero-lag cross-correlation, and we give details of how this error is computed in Appendix A. It should be noted however, that since the estimate of $\hat{\rho}_{FT}(\tau_l)$ depends inversely on the square root of the product of the estimated variances in F and T, any systematic error in these quantities will add to and may exceed the formal errors quoted. This is particularly difficult for the "signal" timing variance, since this is very small and is influenced strongly by the filtering and timing model fitted to the observations. We analyzed the data with polynomials of differing orders and found an increase in the anti-correlation with increasing order of the polynomial, which reduces the estimated timing variance $\hat{Q}_{TT}(0)$.

Having established the existence of variations in flux and TOA on time scales of 10-20 days, we show in Fig. 4 the same data as in Fig. 1, smoothed by a running mean over 20 days. By averaging the day-to-day fluctuations this shows the slow variations much more clearly. An average is calculated for each observed value by adding any other observations that lie within ± 10 days; thus in the plot some average points may correspond to only one observation, others may include 4 or 5 observations. Also shown are running estimates of the rms deviation of the observations in each 20-day window.

3.2. Contribution of ESEs

As noted above, Figs. 1 and 4 include data from the Extreme Scattering Events. In Fig. 4 the time periods of the ESEs are marked by pairs of vertical dotted lines. As can be seen in the October 89 event, the flux decreased smoothly to a minimum

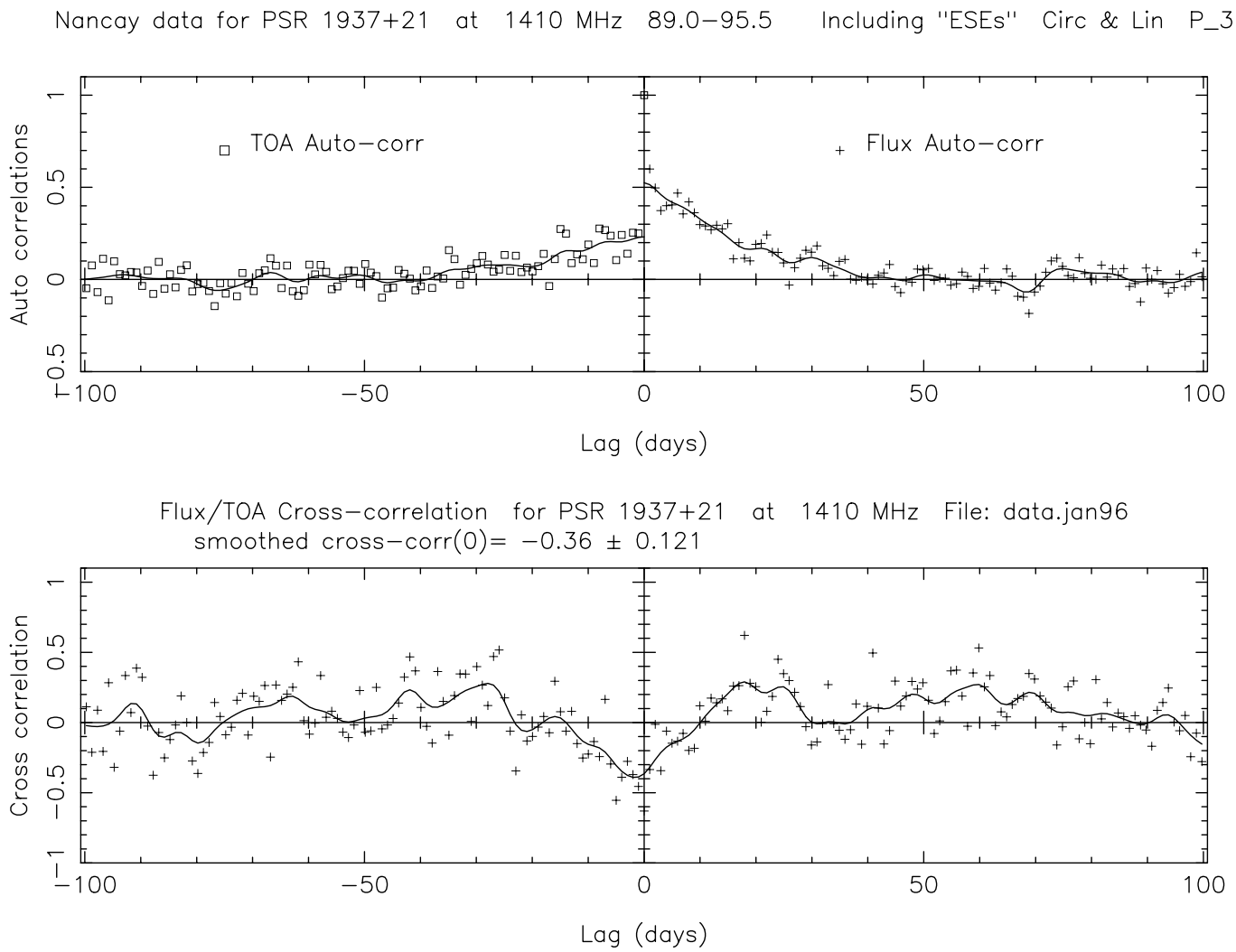

Fig. 3. Auto and Cross correlation functions for the pulse flux and residual TOA at 1.41GHz versus time lag. For the TOA the auto-correlation is displayed for negative time lags. Normalization is described in the text. The solid lines are smoothed versions of the points formed by convolution with a Gaussian function falling to 1/e at 2.5 day, but omitting the zero lag spike in the auto-correlations . All of the data shown in Fig. 1 are included.

Table 2. Cross-correlation analysis of the Flux and TOA residual for two time intervals with and without the Extreme Scattering Events and using 3rd or 5th order polynomials in the TOA fitting model

Dates	ESEs	Polynomial order fitted	ρ_{FT}	m $\sigma_F / < F >$	σ_T μsec
89.0-95.5	included	3	-0.36 $\pm$0.10	0.30 $\pm$0.02	0.27 $\pm$0.1
89.0-95.5	excluded	3	-0.26 $\pm$0.18	0.23 $\pm$0.02	0.27 $\pm$0.1
89.0-92.0	included	3	-0.43 $\pm$0.14	0.30 $\pm$0.03	0.30 $\pm$0.1
89.0-92.0	excluded	3	-0.33 $\pm$0.11	0.23 $\pm$0.02	0.33 $\pm$0.1
89.0-92.0	included	5	-0.73 $\pm$0.29	0.30 $\pm$0.03	0.19 $\pm$0.1
89.0-92.0	excluded	5	-0.60 $\pm$0.25	0.23 $\pm$0.02	0.18 $\pm$0.1

and then increased back to its normal average value. At the same time the pulses were generally late (an increase in TOA), and the TOA also became more variable, as shown in the running rms plot. The other events exhibit the same general features, particularly an inverse relation of flux and TOA. Consequently, we have examined their influence on the cross-correlation function, by excluding the data from the ESEs. The anti-correlation becomes barely significant, being within 1.5 standard errors of zero. As noted above the order of the polynomial in the timing model also has an important influence. In Table 2 we list the zero lag correlation coefficients with and without the five ESE's for the entire data set (89.0-95.5) shown in Fig. 1. We also list the re-

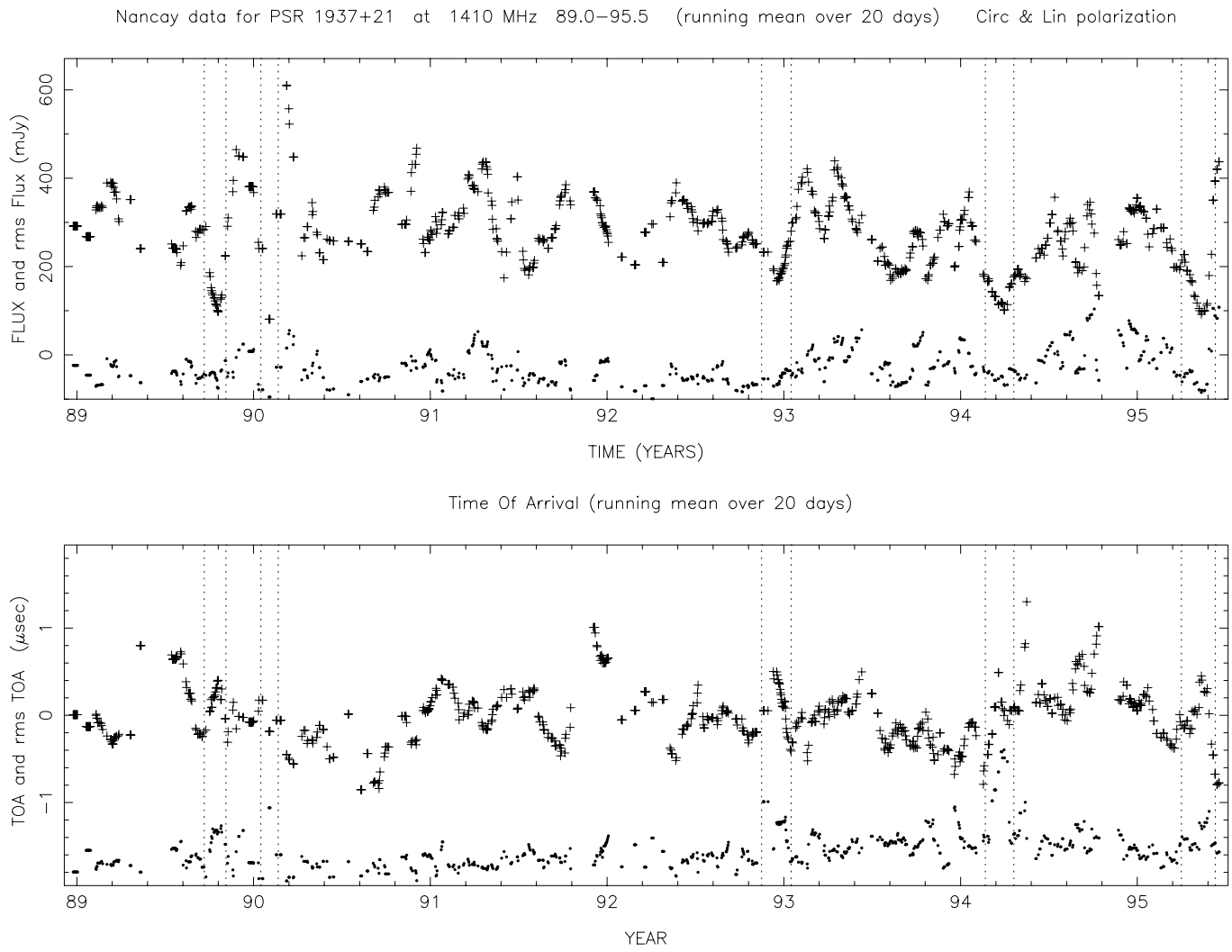

Fig. 4. PSR B1937+214 time series of the pulse flux at 1.41 GHz smoothed by a running mean over 20 days and post-fit residual in the Time of Arrival (TOA), also smoothed by a running mean over 20 days. Below each curve is a display of the running estimate of the rms deviation of the observations inside each 20-day interval, which displays the level of short term variability in the observations. In the rms plots the scales are the same (mJy for the flux and μsec for the TOA), but the zero is the baseline with the horizontal axis. The 5 periods identified as Extreme Scattering Events are indicated by pairs of vertical dotted liness.

sults with and without the two ESEs, for the better quality subset (89.0-92.0), for two polynomial orders. In each case we include the associated estimates of scintillation index and standard deviation in TOA, derived from the smoothed variances $\hat{Q}_{FF}(0)$ and $\hat{Q}_{TT}(0)$. We conclude, from Fig. 3 and Table 2, that the anticorrelation is most evident in the 89.0-92.0 subset of the data, and that "ESE"s dominate the estimated cross-correlation coefficient and have a smaller influence on the smoothed variances.

However, we must question the "ESE" identification and ask whether we have simply selected and removed periods of normal RISS in which the flux decreased more than usual. The criteria for an ESE classification were an unusual increase in the rms TOA as displayed by the lowest plot of Fig. 4 and an associated (smooth) decrease in flux. Since the errors in the TOA estimates vary inversely with the flux, low flux and high rms TOA should be correlated. The lowest flux periods in Fig. 4 are indeed flagged as ESEs and are accompanied by higher rms TOA. However, there is no process that should bias the TOA late when the flux is low as observed. Clearly the anti-correlation of flux and TOA is not an artifact. More questionable is whether the events flagged as ESEs are indeed discrete events or just form a continuum with the other RISS variations.

The October 1989 ESE was, fortuitously, very well sampled and its identification as a discrete event seems secure (Cognard et al., 1993). The chance of catching an event during this period of closely spaced observations is very small, unless such events are relatively frequent for this pulsar. Thus, though the other events are less well observed and their ESE identification could be questioned, we suggest that they too are discrete events and not just unusual periods of normal RISS. In summary, there appears to be a background level of random fluctuations in flux (due to RISS) with discrete interstellar propagation events su-

perimposed, each presumed to be due to a discrete structure passing slowly through the line of sight; these discrete events are characterized by a reduced flux and generally late TOAs. There remains the possibility that the background RISS also causes TOA variations at a level below our errors and that these are anti-correlated with the flux.

4. Interpretation as interstellar scintillation

As discussed in detail below, there is a strong reason to believe that the flux variations are due to Refractive Interstellar Scintillation (RISS). Thus the anticorrelation of TOA variations with the RISS variation labels these TOA variations as interstellar in origin also. However, their association with the ESEs suggests that they are not part of the background RISS phenomenon. The TOA variations are thus important not only for probing the causes of ESEs, but also for possibly reducing part of the TOA variations and so further refining the precision with which the pulses from this and other millisecond pulsars can be timed. In this section we analyse what are the expected auto and cross correlations due to background RISS, with the necessary theory presented as Appendix B. We then consider the implications of the ESEs.

4.1. Flux variations as RISS

Two parameters that can be extracted easily from the autocorrelations of the flux in Fig. 3 are the modulation index and the time scale of their variations. The modulation index $m_{\rm r}$ is the rms variation in flux normalized by the mean flux and was estimated by:

$$m_{\rm r} = \frac{\sqrt{\hat{Q}_{FF}(0)}}{< F >} \tag{9}$$

The time scale $\Delta\tau_{\rm r}$ characterizes the width of the autocorrelation function, and it is defined observationally by the time lag where $\hat{Q}_{FF}(\tau)$ falls to half of its zero lag value. These measured parameters are to be compared with the theory of RISS. In Sect. 4.3 below, we also estimate the cross-correlation of flux across frequency and compare with theory.

The theory of RISS variations, presented by various authors, depends on a detailed model for the spatial and spectral distribution of the interstellar plasma density. The canonical model is that of an isotropic Kolmogorov wavenumber spectrum with an approximately uniform spatial distribution along the line-of-sight from the pulsar. An alternative that is easier mathematically is that the scattering is concentrated in a thin layer, which can be modelled as a thin screen. In view of the evidence for a very clumpy distribution of scattering material in the ISM, the screen model may even be the more realistic. While there is evidence for anisotropy in the scattering on some lines of sight, we expect that random orientations along the line of sight will normally reduce the effective anisotropy.

The RISS modulation index and time scale of several pulsars have been reported by Kaspi & Stinebring (1992), Stinebring et al (1996) & Gupta et al. (1993). We use the theoretical expressions from the latter paper, based on the uniformly distributed Kolmogorov spectral model, to predict theoretical values expected for PSR B1937+214 at 1410 MHz in terms of its diffractive scintillation bandwidth $\Delta\nu_{\rm d}$ as measured by Ryba (1991). Their Eq. (3) with $\Delta\nu_{\rm d}$ = 0.5 MHz at 1410 MHz gives the predicted modulation index $m_{\rm r} = 0.28$. As listed in Table 2 the 89-95.5 1410 MHz observations give $m_{\rm r} = 0.30 \pm .02$, which is in good agreement with the theory.

From Fig. 3 we estimate $\Delta\tau_{\rm r} = 13 \pm 4$ days. Eq. (4) of Gupta et al. (1994) for $\Delta\tau_{\rm r}$ requires estimates for the pulsar distance and the transverse scintillation velocity. We take a distance of 3.6 kpc from the Taylor & Cordes (1993) model. The fitted proper motion (Table 1) gives velocity of 10.5 km/s, which probably underestimates the scintillation velocity, since over 3.6 kpc we expect substantial random velocities of the interstellar plasma and some differential rotation. Adopting a velocity of 50 km/s, in agreement with the measured scintillation velocity from Ryba (1991), we obtain $\Delta\tau_{\rm r} \sim 17$ days. A somewhat simpler theoretical estimate can be made from:

$$\Delta\tau_{\rm r} \sim \sigma_{\rm r}/V = \sigma_{\rm d}/V(r_f/\sigma_{\rm d})^2 \sim \Delta\tau_{\rm d}(\nu/\Delta\nu_{\rm d}). \tag{10}$$

Here $\sigma_{\rm r}$ and $\sigma_{\rm d}$ are the spatial scales of the refractive and diffractive scintillation patterns, respectively. With $\Delta\tau_{\rm d}$ = 7 mins typical of Ryba's measurements, we obtain $\Delta\tau_{\rm r}$ = 14 days, in agreement with the value derived from Fig. 3.

The satisfactory agreement between theory and observation for $m_{\rm r}$ and $\Delta\tau_{\rm r}$ is strong evidence that RISS is indeed responsible for the 10-day variations of flux. We note, however, that the effect of excluding the ESE's makes a significant difference to our observed parameters ($m_{\rm r}$ is reduced by about 20% and $\Delta\tau_{\rm r}$ is nearly doubled with much increased uncertainty). Clearly our RISS model of the interstellar propagation is only approximate. Nevertheless, we now use the Kolmogorov model to predict what TOA variations should be seen and their expected cross-correlation with the RISS modulations of flux.

4.2. The Flux - TOA correlation

The decay in the ACF of the TOA in Fig. 3 has a time scale similar to but somewhat longer than that of the flux. We consider here what TOA variations should be caused by the irregular ISM and whether an anti-correlation with the flux is expected under normal RISS. In our earlier report (LCB) we used the theory of Blandford & Narayan,1985 (BN85) & Romani, Narayan & Blandford,1986 (RNB86) to interpret the anticorrelation and hence constrain the model for the interstellar density spectrum. However, we omitted to account for the partial removal of the DM variations from the TOA's, and we now re-examine the theory.

The intensity and TOA are both influenced by propagation through the irregular interstellar plasma. The primary effect is the phase modulation imposed by the irregular refractive index of the medium. The geometric optics phase is an integral along the line of sight. However, for many purposes its effect can be approximated by considering a phase screen located midway

between source and observer. BN85 used this approximation, which RNB86 validated by a more exact calculation. They introduced the method of intensity-weighting to obtain explicit expressions for the auto and cross correlation of the flux, TOA and other observable quantities. The correlations are given as integrals over the two-dimensional wavenumber (q) of the spectrum of phase fluctuations $P_\phi(q)$, which they modelled as:

$$P_\phi(q) = \lambda^2 Q(q) = \lambda^2 Q_0 q^{-\beta} \tag{11}$$

where β takes the value 11/3 for the Kolmogorov spectrum. Their definition of TOA included the variable dispersive delay, which causes a formal divergence of the integral for the correlation of TOA. They suppressed the divergence by putting a lower wavenumber limit to the integration equal to $(VT_{\rm obs})^{-1}$, where $T_{\rm obs}$ is the total duration of the observations and V is the relative transverse velocity of the observer with respect to the interstellar diffraction pattern. In our observations the dispersive delay is partially removed either by the subtraction of a polynomial fitted to the TOA or by subtraction of a running mean estimate of the dispersive delay from two- frequency observations when available. Either procedure can be modelled as a high-pass filter in the observed frequency domain, but it is not as simple as replacing the lower limit in the two-dimensional wavenumber integration since the filtering is along one wavenumber dimension only.

The primary observations are at a frequency of 1.41 GHz with residual TOA $T(t)$ at epoch t. There are two main propagation contributions expected to $T(t)$: the dispersive plasma delay $T_{\rm D}$ and a refractive delay due to the longer path length of waves refracted from a straight-line path (see BN85), which we call the "geometric delay" (Foster & Cordes, 1990)

$$T(t) = T_{\rm geo}(t) + T_{\rm D}(t) \tag{12}$$

where for very small refraction angles $\theta_{\rm r}$ at distance L

$$T_{\rm geo}(t) = 0.5 L \theta_{\rm r}^2 \tag{13}$$

In our observations $T_{\rm D}(t)$ is partially removed either by subtracting a polynomial timing model fit to the TOA or by subtracting a smoothed estimate of $T_{\rm D}(t)$. We characterize this by the time constant B of the equivalent high pass filter. The resulting TOA residual consists of the geometric delay and the residual dispersive delay. In Appendix B we examine the modification of the RNB86 theory to include only the residual dispersive delays. However, it is instructive to consider the physics of how the two TOA terms are correlated with the flux.

Consider first the geometric delay, which in Appendix B we show is positively but weakly correlated with the flux. Evidently the geometric delay will be greatest when the waves are refracted through the greatest angle, i.e. $|\theta_{\rm r}|$ is a maximum. This condition occurs where the refractive flux curve has its steepest transverse gradient. With the observer's transverse motion through the pattern this condition is typically at neither a maximum nor a minimum flux, and so does not lead to a persistent correlation of TOA and flux. The positive correlation results from the following second order effect. The observed delay is in fact an average of delays from ray paths distributed over a scattering disk. At a refractive flux maximum the ray paths are received from a larger region than at a flux minimum and so there is a larger geometric delay from averaging over the larger region. The lower panels of Fig. A1 plot the theoretical normalized correlation coefficients of flux and $T_{\rm geo}(t)$. Note that the positive correlation remains approximately constant for time lags as large as τ_r.

Now consider the residual dispersive delay. When an increased plasma density region crosses the line of sight it increases the dispersive group delay, but commonly it will also cause a de-focussing of the waves since the plasma refractive index decreases with increasing density. This creates an anti-correlation between flux and $T_{\rm D}(t)$, also shown in the lower panels of Fig. A1. When the two effects are combined (solid curve), there is a net negative peak correlation at zero lag, the magnitude of which depends strongly on the high-pass filter time constant B.

The theoretical normalized correlation functions are given in the upper panels of Fig. A1 and are to be compared with the measured correlations in Fig. 3. The comparison requires a conversion from spatial to temporal lags; so we need the effective velocity V and the refractive scale $\sigma_{\rm r}$, which is also the radius of the scattering disc. However, if we accept that the flux variations are RISS, the scale is set from the auto correlations of flux, and the relative width of the TOA auto correlation can be compared with theory. There is a strong influence of the high-pass time constant, due to the steep power law spectrum of the dispersive TOA fluctuations. As discussed in Appendix B, we estimate $B \sim 100$ days for the polynomial used in the TOA fitting for the data of Fig. 3 and with a refractive time scale of 13 days the ratio $VB/\sigma_{\rm r} \sim 8$, which is shown in the left hand panels of Fig. A1. The time scale for the TOA variations is then substantially longer than the 13 days of the flux variations. Analysis of Fig. 3 can in principle yield an observed time scale for the TOA variations. Using the same procedure as for the flux variations in Fig. 3, we estimate a time scale of 16 ± 10 days. However, we emphasize that the ACF of the TOA is very poorly determined, and depends on the details of the ACF computation. The apparent time scale is increased when the ESE's are removed, since the ESEs include large amplitude rapid variations in the TOA as well as a 10-day modulation anti-correlated with the flux.

The comparison of the theoretical and measured cross-correlation is reasonably satisfactory; a value -0.3 to -0.4 is found from Table 2 and the predicted value is -0.48. However, the large fractional uncertainty in the TOA variance ($\hat{Q}_{TT}(0)$) dominates the uncertainty in the cross correlation coefficient. For example, the effect of reducing B (by fitting a fifth order polynmial) decreases the TOA variance and so boosts the apparent cross correlation coefficient to -0.7, but the errors are proportionately increased also. As further discussed at the end of Appendix B, the observed variance in residual TOA can also be compared with the predicted value. Again the prediction agrees for the nominal conditions but depends strongly on the time constant B.

In summary, we note that the Kolmogorov theory gives a reasonable agreement with the observed parameters for the flux and TOA auto and cross correlations. However, we cannot draw a strong conclusion from the agreement since the Kolmogorov theory has no explanation for the ESE's and for their substantial influence on the observed correlations. Our overall interpretation is that we measure a background level of RISS modulations of the pulsar flux with an added component due to a few discrete events. These events seem to dominate the residual TOA fluctuations on times of 10 to 30 days, making it difficult to identify the weaker ISS modulations of the TOA. The anti-correlation of flux and TOA is to be expected for both the background ISS and for discrete events since they are both due to plasma perturbations in the line of sight. An alternative interpretation, that the ESEs are not discrete events and are just selected portions of the normal RISS, cannot be entirely ruled out. Observationally, both interpretations imply that a significant residual TOA variability is due to variations in the dispersive delay on time scales of 10-20 days that are anti-correlated with the flux variations. From the standpoint of the ISM the alternative interpretation is quite different, since there is no need to invoke the existence of discrete plasma clouds, whose proposed properties are discussed in Sect. 5.

4.3. Correlation of flux over frequency

A further comparison with the Kolmogorov theory can be made for the pair-wise cross-correlation of the multi-frequency flux observations of Fig. 2. The auto and cross correlations are shown in Fig. 5. The auto-correlations of the flux show the same noise spike and slow decay over 10 to 20 days as in Fig. 3. Fig. 5a shows the flux correlations between 1280 and 1410 MHz and Fig. 5b between 1280 and 1700 MHz. There are clear positive cross-correlations centered on zero lag, whose widths are similar to that in the flux ACF of Fig. 3. The zero lag cross-correlation coefficients and errors are given in Table 3, with and without the identified ESE events. Evidently the flux fluctuations are broad-band in nature with and without the ESEs. As discussed in Sect. 2, the multi-frequency observations were linearly polarized and subject to TOA fluctuation noise from random ionospheric Faraday rotation. Consequently, in a correlation analysis of the multi-frequency TOA data, we saw no significant interstellar fluctuations, since they were too small compared with the noise spike. In addition there was no organised correlation detectable between flux and TOA nor between the TOA at pairs of frequencies.

We calculated the theoretical degree of cross-correlation between the flux at the two frequency-pairs, assuming the Kolmogorov spectrum model of the ISM as discussed in the next section. The values are given in Table 3 with the observed values. Both sets of results agree with the theory within the statistical errors. Though they do not constrain the interpretation very strongly, the agreement does confirm that the flux variations are due to interstellar propagation, and that the ESEs are broad band in nature.

Table 3. Cross-correlation analysis of the Flux between pairs of frequencies with and without the Extreme Scattering Events during 92.0 to 95.5.

ν_1 GHz	ν_2 GHz	$\rho_{\rm obs}$ (inc ESEs)	$\rho_{\rm obs}$ (exc ESEs)	$\rho_{\rm theo}$
1.28	1.41	0.986 ± 0.03	0.960 ± 0.03	0.978
1.41	1.70	0.93 ± 0.05	0.93 ± 0.05	0.917
1.28	1.70	0.79 ± 0.1	0.74 ± 0.1	0.834

5. Discussion

We have described flux variations characterized by an rms of 30% over a typical time scale of 13 days. These appear to be a combination of statistically stationary RISS and superimposed a small number of discrete events (ESEs), in which the flux exhibits a relatively smooth minimum over 10 to 30 days. The ESEs also show variations in the TOA with an rms of about 0.3 μsecs which are anti-correlated with the flux; there may also be similar but weaker 0.15 μsecs TOA variations anticorrelated with the background RISS, which are at or below the level of our measurement uncertainties. We now ask what interstellar structures might be responsible.

The background RISS behaviour is entirely consistent with measurements from other pulsars, and is thought to be due to a pervasive distribution of electron density perturbations whose spatial spectrum follows the Kolmogorov spectrum over at least six orders of magnitude (Armstrong at al. 1995). By contrast models for ESEs are more tentative. In the paper reporting the first such event, Fiedler et al. (1987) proposed that it was caused by the intervention in the line of sight of a discrete dense region of plasma with small scale irregularities whose enhanced scattering was responsible for decreasing the source flux by about 40%; hence the name Extreme Scattering Event. An alternative model, proposed by Romani et al. 1987, argues that the events are also due to a discrete dense region of plasma, which instead acts as a diverging lens in reducing the observed flux. In the paper reporting the Oct 1989 ESE from PSR B1937+214, C93 presented such a model of enhanced refraction for the event. Simonetti (1991) constructed a similar model in attempt to model a large swing in polarization angle observed in quasar 0917+624. Typically such models must have a dimension on the order of a few astronomical units and an electron density of ≥ 100 cm^{-3}. For temperatures near 10^4K such densities imply a pressure more than 100 times greater than typical interstellar pressures (Kulkarni & Heiles, 1986), which creates a problem in explaining their origin. Romani et al. 1987 also suggested non-spherical models (such as sheets or filaments), which can reduce the required electron density, and they also proposed confinement by the enhanced pressure in an expanding supernova shell. Clegg et al. (1988) analysed models of interstellar shocks due to supernovae and stellar winds as potential lensing structures.

In applying these ideas to our observations of PSR B1937+214, we have the added information from multiple events, giving information on the space density of the objects responsible. We take the results from the October 89 event as

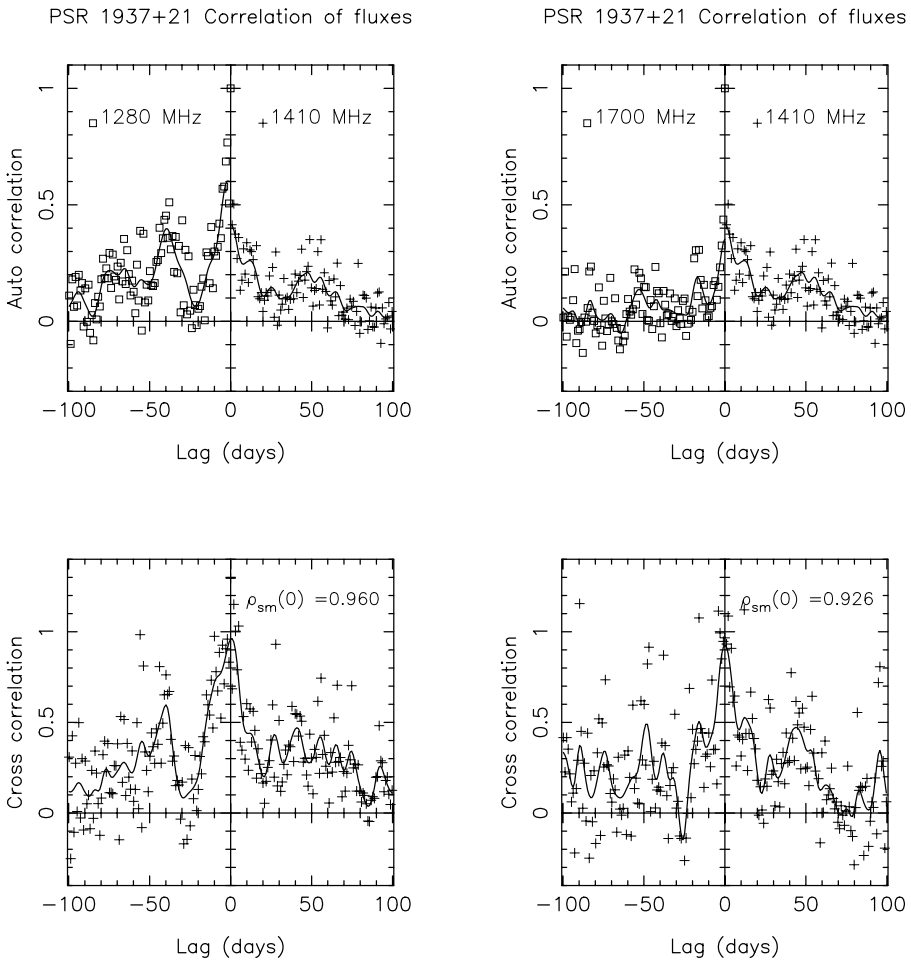

Fig. 5. Auto and Cross correlation functions for the pulse fluxes at pairs of frequency for the data from Fig. 2 (including ESEs). Normalization corrects for the noise contributions as described in the text. The solid lines are smoothed versions of the points formed by convolution with a Gaussian function falling to 1/e at 2.5 day, but omitting the zero lag spike in the auto-correlations.

typical of the others. The event duration $T_{\rm ese} \sim 20$ days yields an approximate transverse scale $a_t \sim VT_{\rm ese} \sim 0.6$ AU, assuming the velocity to be 50 km/s as before. With 5 events, for a total of about 100 days, observed in 6.5 years, we estimate the probability of an event to be 0.042.

Another type of transient propagation event has been seen in the diffractive scintillation spectra of pulsars, in which fringes are observed to modulate the spectrum for similar episodes of 10-30 days. These have been called multiple imaging or interstellar fringing events (Hewish et al. 1985, Cordes & Wolszczan 1986, Wolszczan & Cordes, 1987, Rickett et al. 1997) and are likely to be caused by the same agent as for the ESEs. Calculations of the possible plasma structures reach similar models for their electron density and size, with similar problems in explaining the stability of such structures in which the pressure is more than 100 times the typical interstellar pressure.

Rickett et al. (1997) proposed a solution to the pressure problem by postulating a layer with multiple weaker density enhancements (~ 0.2 cm^{-3}) in the form of sheets or filaments of thickness on the order of 1 AU, in approximately normal interstellar pressure balance. The associated refraction was normally small enough not to cause amplitude modulation. On rare occasions, however, the refraction angle was sufficient to cause the fringing and perhaps the amplitude modulation comparable to that in an ESE. This layer was proposed to coexist with the more pervasive interstellar distribution of turbulent plasma. In trying to apply this model to our observations we conclude that it would predict too high a level of background amplitude fluctuations to be compatible with the observations. We need a model which contributes amplitude modulation only in the form of the discrete events. Consequently we assume a discrete refracting "cloud" for each event, as in previous ESE models.

So now consider a distribution of sheet-like or filamentary clouds of electron density $\delta N_{\rm e}$ with smallest dimension $\sim a_t$ and greatest dimension a factor η larger. Let there be $n_{\rm sh}$ sheets or $n_{\rm fi}$ filaments per unit volume randomly distributed over the entire line of sight (L). Then the probability of a single intersection favourably oriented (parallel) with the line of sight is:

$$M_{\parallel,sh} \sim n_{\rm sh} L a_t^2 \quad M_{\parallel,fi} \sim n_{\rm fi} L a_t^2/\eta^2. \tag{14}$$

In each case we equate this probability to our estimate of 0.04 and using a_t we obtain $n_{\rm sh} \sim 4 \times 10^{-44}$m^{-3}. This is 10^6pc^{-3} and suggests 1-AU size plasma clouds that are over a million times more common than stars. For filaments their number density $n_{\rm fi}$ would be a factor η^2 larger.

During the occasional alignments of their long dimension along the line of sight the angles of refraction will be given by $\theta_\parallel \sim \lambda^2 r_{\rm e} \delta N_{\rm e} \eta / 2\pi$ for either a sheet or a filament. The

condition for the large amplitude modulation (sometimes called the multipath condition) is overlap between the refracted and unrefracted raypaths. This depends on the distance $L_o = xL$ from the observer to the cloud and gives:

$$Lx(1-x)\lambda^2 r_e \delta N_e \eta/2\pi \sim a_t \quad (15)$$

which for our observations of PSR B1937+214 ($\lambda = 21$ cm, L = 3.6 kpc) becomes:

$$\delta N_e \eta x(1-x) \sim 46 \mathrm{cm}^{-3} . \quad (16)$$

Since $x(1-x) \leq 0.25$, the lowest electron density for isotropic clouds ($\eta \sim 1$) would then be about 200 cm^{-3}, comparable to other ESE models. Eq. (15) is the same condition as that given in other analyses (eg Clegg et al. 1988).

We have now to consider the "non-aligned" intersections and whether they cause significant amplitude modulation. These occur for sheets or filaments approximately perpendicular to the line of sight. The chance of such alignments will be $M_{\mathrm{sh},\perp} \sim \eta^2 M_{\mathrm{sh}\|}$ for sheets and $M_{\mathrm{fi},\perp} \sim \eta^3 M_{\mathrm{fi}\|}$ for filaments. These M-values may well be greater than unity, in which case they represent the typical number of intersections for a single observation, which add incoherently. The associated angles of refraction are

$$\theta_{sh,\perp} \sim \theta_\| \sqrt{m_{\mathrm{sh},\perp}}/\eta^2 \quad (17)$$

where $m_{\mathrm{sh},\perp}$ is taken as the maximum of 1 and $M_{\mathrm{sh},\perp}$. For filaments the relations are

$$\theta_{fi,\perp} \sim \theta_\| \sqrt{m_{\mathrm{fi},\perp}}/\eta, \quad (18)$$

with a similar interpretation of $m_{\mathrm{fi},\perp}$. Using ray concepts again, we estimate the fractional variation in flux by $x(1-x)L\partial\theta/\partial\xi$, where ξ is a transverse spatial coordinate. The multipath condition (eqn 15) sets this to be typically about unity for the *favourable* intersections. Hence, we can find that for the *unfavourable* intersections (after simplification):

$$\Delta I/I|_{sh,\perp} \sim \max[0.2/\eta^2, 1/\eta^3] \quad (19)$$

and

$$\Delta I/I|_{fi,\perp} \sim \max[0.2\eta^{0.5}, 1/\eta] \quad (20)$$

An examination of these equations shows that the filaments must give significant persistent intensity fluctuations for all values of η, having a minimum of 34% for $\eta \sim 2.9$. By contrast, the sheets give only weak fluctuations, being less than 10% for all $\eta > 2$. Consequently, we propose that the ESEs are due to de-focussing events from refracting sheets of plasma of thickness ~ 0.6 AU, when they are aligned parallel to the line of sight. By increasing their "axial ratio" η we can reduce the required electron density in the clouds and at the same time suppress the level of more frequent amplitude fluctuations caused by perpendicular intersections.

A further observed quantity is the extra delay caused when a plasma sheet causes a parallel intersection. For the Oct 89 event we observed TOA fluctuations of $1\pm1\mu$sec, to which were fitted a two-part density profile, that followed the major TOA perturbation. In terms of the model presented here, we simply estimate the delay due to parallel alignments and compare with the typical delay of 1 μsec. There are dispersive delays $\tau_{\delta\mathrm{DM}}$ and geometric delays τ_{geo}, but for a de-focussing event the two terms must be approximately equal, in accord with Fermat's principle. The former gives $\tau_{\delta\mathrm{DM}} \sim \lambda^2 r_e \delta N_e a_t \eta/(2\pi c)$, which we note approximates the geometric delay $a_t\theta_\|/c$. The interference condition, Eq. (15), allows this to be expressed as:

$$\tau_{\delta\mathrm{DM}} \sim a_t^2/cLx(1-x) \geq 1.2\mu\mathrm{secs}. \quad (21)$$

The close agreement with the typical observed delay supports our interpretation of the ESEs as de-focussing events, (as already demonstrated in the more detailed analysis of C93).

Of course, we have not proven that the sheet scenario is the correct interpretation, simply that it is consistent with the observations. We can also consider other geometries. Initially we assumed that the sheets were distributed randomly over the entire path length and found their space density to be about 10^6 pc^{-3}. Though this seems large, the distribution seems sparse when the typical spacing between the sheets is compared to their largest dimension ($a_t\eta$). The density $n_{\mathrm{sh}} \sim 4\times10^{-44}$m^{-3} corresponds to a typical spacing of 3×10^{14}m or about $3000a_t$. According to the scenario analysed above the sheets are completely independent of each other, unless the axial ratio approaches the unreasonably large value of 3000.

Alternatively, we can consider the sheets to be connected - making a network or "foam". If the foam were confined in a layer of thickness D and had plane randomly oriented faces (a_t thick), we find the probablity of an aligned intersection to be $\sim 3D/(a_t\eta^3)$ which we can equate to the observed 0.04. We must have $L \geq D \geq \eta a_t$ which gives $3000 \geq \eta \geq 9$. Since axial ratios larger than about 20 must be relatively rare, such a foam model is more reasonable if it is confined to a layer with only a few cells thick and does not extend through the entire ISM. Such an idea is consistent with the inhomogeneous nature of the ionized ISM, as discussed by Kulkarni & Heiles (1986), who estimate a filling factor of 10% for the Warm Interstellar Medium (WIM). Another possibility is for the faces to be irregularly curved with a typical radius of curvature R_c. Clegg et al. (1988) suggested that such distortions in supernovae shells would be common due to the swept up neutral HI clouds. The effective axial ratio of a curved surface of thickness a_t is $\sqrt{2R_c/a_t}$, but the length of the sheets could be substantially larger than ηa_t and such a foam could, in principle, extend over most of the distance to the pulsar.

We now must ask what astronomical structures are responsible. The model of isolated 0.6AU spherical clouds requires too many clouds of too great an electron density. Sheetlike clouds (with axial ratio ≤ 20) require a lower density (10 electrons cm^{-3}) and could be confined to one tenth of the pulsar distance (0.4 kpc), which could be substructure in the warm ionized regions probed by Hα observations (eg Reynolds 1991). If the sheets are in thinner layers they could be partially or completely connected; thus maybe they could be the outer ionized envelopes to neutral HI clouds, especially near an ionizing stellar source whose radiation only penetrates partially into the HI. Sheetlike and filamentary structures have been proposed by

Heiles (1997) to explain the smallest scale (30AU "tiny scale") structures observed in HI, which he interprets as cool (15 K) elongated or flattened clouds in normal pressure balance. However, his estimated electron density is much too small to cause the ESEs. They are embedded in warmer less dense regions, and we wonder if their outer envelopes may in some circumstances be ionized and form the proposed thin ionized sheets.

Other connected sheet structures are possible in shock fronts associated with expanding shells due to novae or stellar winds. A system of supernovae superbubbles has dimensions too large for a connected sheet (foam) model. However, if the line of sight happens to be parallel to and pass through a single supernova shell the multiple events could be explained as various quasi-parallel but disjoint subsections of the shell which happen to line up as they pass in front of the pulsar. The mean time of 1.3 years between the events would correspond to transverse separations of about 13 AU (at 50 km/s). Of course this scenario presupposes that the line of sight to PSR B1937+214 is special and that the frequent ESEs are a phenomenon special for this pulsar. We note that a small remnant G57.2+0.8, only about one degree from the pulsar (Sieber & Seiradakis, 1984), as listed in the catalog of D.Green, 1997. Fiedler et al. (1994) suggested that the remnants responsible for the ridges of emission seen in low frequency radio maps may be responsible for the ESEs reported in extragalactic radio sources. This model is similar to that of Romani et al. (1987) and has the advantage of a specific source of the necessary extra pressure in the form of the supernova blastwave.

6. Conclusions

1) We have observed TOA variations in the millisecond pulsar B1937+214 that are interstellar in origin and which fluctuate over times of 10 to 30 days. The TOA is generally delayed and variable during the periods when the radio flux exhibits a smooth minimum. We have classified these times as discrete events (ESEs) and observed 5 of them in 6 years of obervations, which gives an event probability of about 0.04.

2) The smooth minima in the flux, described in (1), are superimposed on a background of stochastic variations in the pulsar flux whose properties (rms and time scale) agree well with those predicted for RISS from the Kolmogorov model of the interstellar plasma density spectrum. With the ESEs removed the expected TOA fluctuations associated with RISS are not definitively detected since their expected level is near our detection threshold.

3) We propose that the ESEs are caused when sheets of enhanced plasma density pass in front of the pulsar and happen to be aligned with the line of sight. Filamentary structures are not suggested since the level of amplitude modulation expected for the more frequent perpendicular intersections is not seen. The time scales suggest a transverse dimension of about 0.6 AU and length perhaps 10 times greater. The product $\delta N_{\rm e}\eta \sim 200{\rm cm}^{-3}$.

4) Possible sites for such structures include the envelopes of neutral HI clouds, the warm ionized medium, shock fronts associated with stellar winds, novae; such models are generic and suggest that other pulsars should show similar events. A more specialized model assumes that the PSR B1937+214 line of sight passes tangentially through a single supernova shell, whose surface is broken or distorted into quasi-parallel sheets, responsible for each event.

5) Though our interpretaion is that the ESEs are indeed discrete events, there remains some doubt that they really are distinct from the background fluctuations. Thus an alternative interpretation of our results is that we have detected an anti-correlation of RISS flux and TOA, due to changes in dispersive delay from small scale plasma structures, which are part of the basic turbulent spectrum, as discussed in Appendix B.

Acknowledgements. We thank J.-P. Drouhin, D. Aubry, B. Darchy at Nançay and F. Biraud at Meudon for their help and insights at various stages of this project. We also acknowledge the many contributions to this project of G. Bourgois, who is now sadly deceased. We thank G. Fréon and the Laboratoire Primaire du Temps et Fréquence (LPTF) at the Observatoire de Paris, for daily UTC corrections between the station clock at Nançay and the conventional UTC time scale. The Nançay Radio Observatory is the Unité Scientifique de Nançay of the Observatoire de Paris, associated as Unité de Service et de Recherche (USR) No. B704 to the French Centre National de la Recherche Scientifique (CNRS). The Nançay Observatory also gratefully acknowledges the financial support of the Conseil Régional of the Région Centre in France. BJR gratefully acknowledges the hospitality of the Observatory at Meudon and support by the NSF under grant AST-9414144.

Appendix A: error analysis for the correlation functions

For small fractional errors in the three quantities in Eq. (8), the fractional error in $\hat{\rho}_{FT}(\tau = 0)$ can be found approximately from:

$$\frac{\sigma_\rho^2}{\rho^2} \approx \frac{\sigma_{R_{FT}}^2}{R_{FT}^2} + 0.25\frac{\sigma_{Q_{FF}}^2}{Q_{FF}^2} + 0.25\frac{\sigma_{Q_{TT}}^2}{Q_{TT}^2} \tag{A1}$$

We estimated the three contributing variances by considering independent contributions from estimation error and from noise. Thus:

$$\sigma_{R_{FT}}^2 \approx \frac{C_{FT}^2}{N_s} + \frac{R_{nF}R_{nT}}{N_n} \tag{A2}$$

Here N_s is the number of independent signal time-scales averaged and N_n is the number of independent noise samples averaged (which is the number of observations times 5 for the gaussian smoothing function used). Similarly:

$$\sigma_{Q_{FF}}^2 \approx \frac{Q_{FF}^2}{N_s} + \frac{R_{nF}^2}{N_n} \tag{A3}$$

and

$$\sigma_{Q_{TT}}^2 \approx \frac{Q_{TT}^2}{N_s} + \frac{R_{nT}^2}{N_n}. \tag{A4}$$

An alternative estimate can also be made of the error in $\hat{\rho}_{FT}(\tau = 0)$, from the rms variation in $\hat{\rho}_{FT}(\tau)$ at time lags substantially greater than the 20 day time-scale of the scintillation process. We used both methods and list in Table 2 the larger of the two.

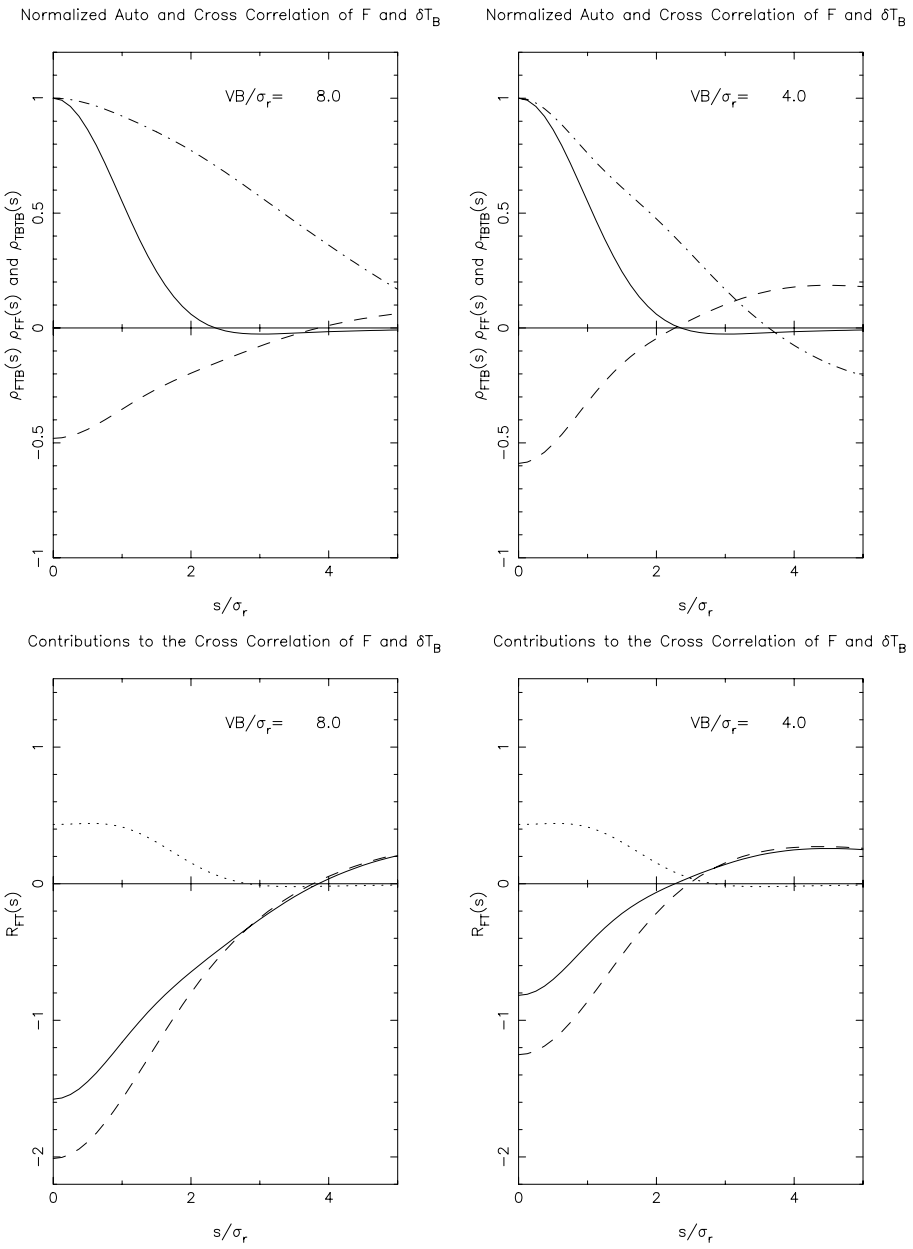

Fig. A1. Theoretical Auto and Cross correlation functions for flux δF and residual TOA δT_B (with dispersive delay partially removed by a running mean over time constant B). s is the spatial offset, $\sigma_{\rm r}$ is the radius if the scattering disc, V is the velocity of the scintillation pattern across the earth. The theory used is an equivalent screen with a Kolmogorov phase spectrum, as described in Appendix B. The top panels give the normalized auto-correlations for flux (solid line), and residual TOA (dash-dot), and the normalized cross-correlation between them (dashed line). The lower panels give the covariance between flux and TOA (solid line), and their break-down into the positive correlation of flux with geometric delay $T_{\rm geo}$ (dotted line) and the negative correlation of flux with residual dispersive delay δT_B (dashed line). The left panel is evaluated for the nominal ratio of the running mean time constant to the refractive scintillation time $= B/\tau_r$; the right panels for the ratio reduced by a factor two.

Appendix B: theory for RISS flux and corrected TOA

We give details of how the theory developed by BN85 and RNB86 can be modified to account for a partial correction of the dispersive delay. We call such an estimate the *corrected* TOA. Eq. (12) gives the TOA variation as the sum of two terms, corresponding to Eq. BN85(3.10); the second term is the variation in the dispersive delay from the assumed constant DM value. It changes as the column density of electrons in the line of sight changes due to relative motion of the pulsar, the interstellar electrons and the earth. The variation is slow and has a very "red" spectrum. In the measurements by KTR94, it was dominated by a slow linear decrease for years 85-92.

In the data of Fig. 1, the slow changes in TOA are "absorbed" by the timing model which was fitted to the arrival times - a third order polynomial and annual terms due to a priori positional errors. This is approximately equivalent to a high pass filter, i.e. subtraction of a running mean. We model the running mean as a convolution of the TOA with a Gaussian function of time, whose width is parameterized by FWHM=$1.66B$. For the data of Fig. 1 we estimate the effective $B \sim 100$ d. In reference to Eq. (12) $T_{{\rm D},B}(t)$ is the mean dispersive delay (smoothed over B), which was subtracted to give the corrected TOA. The variations in $T_{\rm geo}$ are faster and essentially unaffected by the high-pass filter. Thus the corrected TOA can be written as:

$$\Delta T_B(t) = T(t) - T_{{\rm D},B}(t) = T_{\rm geo}(t) + \Delta T_{{\rm D},B}(t) \qquad \text{(B1)}$$

where the more rapid dispersive variations are written as:

$$\Delta T_{{\rm D},B}(t) = T_{\rm D}(t) - T_{{\rm D},B}(t). \qquad \text{(B2)}$$

In describing the theory we use the δ-notation of BN85 for normalized fluctuations and write their Eq. (3.12) for the normalized TOA fluctuation as:

$$\delta T = \delta T_{\rm D} + \delta\Omega \tag{B3}$$

where $\delta\Omega = T_{\rm geo}/\Delta\tau_{\rm d}$ is the normalized geometric delay, which is the same as the fluctuation in solid angle given by their Eq. (3.8) and $\Delta\tau_{\rm d}$ is the diffractive broadening time used as the normalizing time constant. Our *normalized corrected* TOA is then:

$$\delta T_B(t) = \delta\Omega(t) + \delta T_{{\rm D},B}(t), \tag{B4}$$

where the second term is the normalized residual dispersive delay that passes the high-pass filter.

BN85 and RNB86 give expressions for correlations of $\delta\Omega$ with δF (the flux normalized by its mean), and we present here comparable expressions for the correlation with the *corrected* TOA. The normalized correlations are displayed in the upper panels of Fig. A1, which should be compared with the measured correlation plots in Fig. 3. The curves are the normalized autocorrelation of flux (solid curve), the normalized autocorrelation of corrected TOA, and the cross correlation of flux and corrected TOA. The theoretical curves depend on the ratio B/τ_r, where τ_r is the temporal scale (at 1/e) of the refractive scintillation pattern, which is also $VB/\sigma_{\rm r}$ with $\sigma_{\rm r}$ defined as the radius of the scattering disc or refractive scale and V as the velocity of the scintillation pattern. The left hand panel approximates the condition applicable to the observations. The flux is anticorrelated with the TOA as observed, with a maximum negative correlation coefficient that depends on B/τ_r. As shown by the lower panels of Fig. 6, this negative correlation is the summation of a positive correlation of flux with geometric delay and negative correlation with the residual dispersive delay, whose amplitude decreases as we decrease B. There is not an exact correspondence between the theory of Fig. 6 and the measurements of Fig. 3. In particular the width and amplitude of the autocorrelations of TOA in Fig. 3 match more nearly with the right hand panels in Fig. 6 than with the left hand panels, which should properly describe the filtering done in the analysis. However, we have already noted the large uncertainties in estimating the ACF of the corrected TOA. Further we must emphasize that this theory does not include any discrete structures in the line of sight, which are needed to explain the ESEs. Nevertheless, we now proceed with details of the theory for a pure Kolmogorov medium.

We are concerned with two normalized variables, $\delta T_B(t)$ the corrected TOA defined above and $\delta F(t)$ the flux normalized by its mean. We follow closely the method of BN85 and RNB86, in which each observable is given as a spatial convolution of a weighting function with the phase from the medium/screen. In the wavenumber domain the convolution becomes the product of the phase spectrum $\phi(q)$ and the corresponding wavenumber filter. For the dispersive delay the filter $f_{\rm D}(q) = 2L/(k\sigma_{\rm r}^2)\exp(-q^2\sigma_{\rm r}^2/4)$ is just the first of the three terms in Eq. (4.11) of BN85. The effect of our one-dimensional Gaussian smoothing of the fluctuation in dispersive delay can then be written as:

$$\delta T_{{\rm D},B}(x) =$$

$$\int_0^\infty \int_0^{2\pi} f_{\rm D}(q)\phi(\mathbf{q}) \left\{1.0 - \exp[-(0.5qVB\cos\theta)^2]\right\}$$

$$\times \exp[iqx\cos\theta] d\theta\ q\ {\rm d}q\ /(4\pi^2) \tag{B5}$$

The temporal variations are found by mapping the component x of the spatial variable to Vt.

For the data we computed the auto and cross correlations of the time series for $\delta F(t)$ and $\delta T_{\rm B}(t)$. There are three correlations involving the flux and TOA, which comprise several contributions written in terms of a spatial offset $\mathbf{s}$ parallel to $\mathbf{V}$. Using Eq. (B4) we obtain:

$$R_{F,F}(s) = < \delta F(\mathbf{x})\delta F(\mathbf{x}+\mathbf{s}) > \tag{B6}$$

$$\begin{aligned} R_{F,TB}(s) &= < \delta F(\mathbf{x})\delta T_B(\mathbf{x}+\mathbf{s}) > = R_{F,\Omega}(s) + R_{F,{\rm D}B}(s) \\ &= < \delta F(\mathbf{x})\delta T_{{\rm D},B}(\mathbf{x}+\mathbf{s}) > + < \delta F(\mathbf{x})\delta\Omega(\mathbf{x}+\mathbf{s}) > \end{aligned} \tag{B7}$$

$$\begin{aligned} R_{TB,TB}(s) &= < \delta T_B(\mathbf{x})\delta T_B(\mathbf{x}+\mathbf{s}) > \\ &= R_{{\rm D}B,{\rm D}B}(s) + 2\ R_{\Omega,{\rm D}B}(s) + R_{\Omega,\Omega}(s) \end{aligned} \tag{B8}$$

The factor 2 in Eq. (B8) results because the correlation $R_{\Omega,{\rm D}B}(s)$ is symmetric in s. In (B6)-(B8) three of the six correlations do not depend on B and are given by BN85 (Appendix B): $R_{F,F}$ $R_{F,\Omega}$ and $R_{\Omega,\Omega}$. We now consider the remaining 3.

Using Eq. (B5) we can write $R_{F,{\rm D}B}(s)$ as:

$$R_{F,{\rm D}B}(s) =$$

$$k^{-2}\int_0^\infty Q(q)\ f_F(q) f_{\rm D}(q) G_{{\rm D},B}(q) q\ {\rm d}q\ /(2\pi) \tag{B9}$$

where:

$$\begin{aligned} G_{{\rm D},B}(q) &= \int_0^{2\pi} \left\{1.0 - \exp[-(0.5qVB\cos\theta)^2]\right\} \\ &\quad \exp[-iqs\cos\theta]{\rm d}\theta\ /(2\pi) \end{aligned} \tag{B10}$$

and $f_F(q)$ is given by eqn (4.9) of BN85, in which $\sigma_{\rm r}$ is the radius of the scattering disc at the equivalent thin screen whose distance is L; thus $\sigma_{\rm r} = L\theta_{\rm d}$ with $\theta_{\rm d}$ as the radius of the scattered angular spectrum. We factor $\exp[-(0.5qVB)^2]$ out of the Gaussian in $\cos^2\theta$ and expand the remaining exponential $\exp(0.5qVB\sin\theta)^2$ as a power series and integrate term by term. Eq. (B10) then becomes:

$$\begin{aligned} G_{{\rm D},B}(q) &= J_0(qs) - \Sigma_{a=0}^{\infty} \frac{1.3...(2a-1)}{a!} \times \\ &\quad \left(\frac{(VB)^2 q}{4s\sigma_B}\right)^a J_a(qs) \end{aligned} \tag{B11}$$

where $\sigma_B^2 = \sigma^2 + 0.5(VB)^2$

In applying (B11) to (B9) we obtain a summation of q-integrals, which yield confluent hypergeometric functions. Following the notation of RNB86, we introduce the functions $h_p^a(s)$ from their Eq. (2.11). Then the sum of q-integrals can be expressed in terms of the following function:

$$H_m[r,u] \;=\; u^{4-\beta+2m}\Sigma_{a=0}^{\infty}\frac{1.3...(2a-1)}{a!}\left(\frac{1-u^2}{2\sqrt{2}}\right)^a \times r^{-a}\; h^a_{m+a/2}(s=u\sqrt{2}r\sigma_{\rm r}) \qquad \text{(B12)}$$

The result is:

$$R_{F,{\rm D}B}(s) = -2K\; h_0^0\left(\frac{s}{\sqrt{2}\sigma_{\rm r}}\right)+2K\; H_0\left[\frac{s}{\sqrt{2}\sigma_{\rm r}},\frac{\sigma_{\rm r}}{\sigma_B}\right] \qquad \text{(B13)}$$

Here the constant K characterizes refractive intensity variance and is given by Eq. (2.14) of RNB86. In completing the q-integral we have to specify limits on the exponent β. The most restrictive requirement comes from the leading terms which give J_0 functions. These two evaluated individually require $\beta < 4$, to avoid a divergence at q=0. However, taken together they converge under the less restrictive condition $\beta < 6$, which is the same condition for the convergence of the a=1 term in the summation, so the net result is correctly given by Eq. (B13) provided $\beta < 6$.

The procedure for $R_{\Omega,{\rm D}B}$ is entirely similar since the filter function for Ω (see BN85 Eq. 4.10) is the same as for F with an added term proportional to q^4. The result is

$$R_{F,\Omega}(s) \;=\; R_{F,{\rm D}B}(s) + 0.5K\; h_1^0\left(\frac{s}{\sqrt{2}\sigma_{\rm r}}\right) - 0.5K\; H_1\left[\frac{s}{\sqrt{2}\sigma_{\rm r}},\frac{\sigma_{\rm r}}{\sigma_B}\right] \qquad \text{(B14)}$$

Finally consider $R_{{\rm D}B,{\rm D}B}$ as

$$R_{{\rm D}B,{\rm D}B}(s) =$$

$$\int_0^\infty Q(q)[f_{\rm D}(q)]^2\left\{1.0-\exp[-(0.5qVB\cos\theta)^2]\right\}^2$$

$$\times\exp[-iqs\cos\theta]{\rm d}\theta\;/(2\pi)q\;{\rm d}q\;/(2\pi k^4) \qquad \text{(B15)}$$

We follow the same general method as above and obtain the following

$$R_{{\rm D}B,{\rm D}B}(s) \;=\; 4Kh_{-1}^0\left(\frac{s}{\sqrt{2}\sigma_{\rm r}}\right) - 8K\; H_{-1}\left[\frac{s}{\sqrt{2}\sigma_{\rm r}},\frac{\sigma_{\rm r}}{\sigma_B}\right] + 4K\; H_{-1}\left[\frac{s}{\sqrt{2}\sigma_{\rm r}},\frac{\sigma_{\rm r}}{\sigma_{B1}}\right] \qquad \text{(B16)}$$

where $\sigma_{B1}^2 = \sigma_{\rm r}^2 + (VB)^2$.

Fig. 6 shows separately the contributions to the cross correlation of flux and corrected TOA , from the geometric delay (dotted line) and the residual dispersive delay (dashed line), together with the total corrected TOA (solid line). The curves are plotted with the constant K set to 1. They reveal how the overall negative correlation is the summation of a positive correlation due to the geometric term and a larger negative correlation due to the dispersive term.

The autocorrelations in the upper panels of Fig. 6 are normalized to unity by dividing by the appropriate variance. The variance of F is the square of the scintillation index, the theory for which was discussed in Sect. (4.1). The variance for the corrected TOA ΔT_B is given by the zero lag value $R_{TB,TB}(0)$.

$$< \Delta T_B^2 >= \Delta\tau_{\rm d}^2 < \delta T_B^2 >= \Delta\tau_{\rm d}^2\; R_{TB,TB}(0) \qquad \text{(B17)}$$

where the latter quantity is obtained from eqn (B8) with $s = 0$. In obtaining a numerical value we need the correct value for the constant K. Via a rather tortuous path through the equations of BN85 or RNB86 this constant can be reduced to:

$$K = A(s_0/r_f)^{8-2\beta} \qquad \text{(B18)}$$

where $r_f = \sqrt{L/k}$ and s_0 if the diffractive scale at the observer and A is a constant that depends only on β. The quantity r_f/s_0 is a strength of scattering parameter, which can be estimated from the diffractive scintillation bandwidth, using the equivalent screen formula:

$$\nu/\Delta\nu_{\rm d} \approx (r_f/s_0)^2 \qquad \text{(B19)}$$

With $\beta = 11/3$ we find

$$K = 0.64(\Delta\nu_{\rm d}/\nu)^{0.33}, \qquad \text{(B20)}$$

which gives

$$< \Delta T_B^2 >\approx 0.0046 R_{TB,TB}(0) \approx 0.05\mu{\rm secs}^2 \qquad \text{(B21)}$$

with B/τ_r = 8.0. We note that the variance 0.05 μsecs^2 gives an rms deviation $\sigma_T \sim 0.22$ μsecs, which is similar to the observed values listed in the last column of Table 2. The good agreement is encouraging, but may be fortuitous, since there are several uncertainties in predicted value as well as in the measured value.

It should certainly be noted that all of the theory in this appendix ignores the effect of discrete scatterers invoked to account for the extreme scattering events.

References

Armstrong J.W., Rickett B.J., Spangler S.R., 1995, ApJ 443, 209

Backer D.C., Kulkarni S.R., Heiles C., et al., 1982, Nat 300, 615

Blandford R.D., Narayan R., 1985, MNRAS 213, 591-611 [BN]

Clegg A.W., Chernoff D.F., Cordes J.M., 1988, in Cordes J.M., Rickett B.J., Backer D.C., (eds), "Radio Wave Scattering in the Interstellar Medium", AIP Conference Proceedings 174, p. 74

Cognard I., Bourgois G., Lestrade J-F., et al., 1993, Nat 366, 320-322 [C93].

Cognard I., Bourgois G., Lestrade J-F., et al., 1995, A&A 296, 169-179 [C95]

Cognard I., Lestrade J-F., 1996, Proceedings of IAU Symp 160, Sydney, Austr., A.S.P. Conference Series 105, 469

Cordes J.M., Pidwerbetsky A., Lovelace R.V.E., 1986, ApJ 310, 737 [CPL]

Cordes J.M., Wolszczan A., 1986, ApJ 307, L27

Cordes J.M., Wolszczan A., Dewey R.J., Blaskiewicz M., Stinebring D.R., 1990, ApJ 349, 245

Fiedler R.L., Dennison B., Johnston K.J., Hewish A., 1987, Nat 326, 675
Fiedler R.L., Dennison B., Johnston K.J., Waltman E.B., 1994, ApJ 430, 581
Foster R.S., Cordes J.M., 1990, ApJ 364, 123
Fukushima T., 1988, in J. Kovalevsky et al. (eds) "Proceedings of Symposium on Reference Frames", Kluwer Academic Publishers, p. 417
Green D.A., 1997, "Catalog of Galactic Supernova Remnants", http://www.mrao.cam.ac.uk/surveys/snrs/snrs.info.html
Gupta Y., Rickett B.J., Coles W.A., 1993, ApJ 403, 183
Gupta Y., Rickett B.J., Lyne A., 1994, MNRAS 269, 1035
Heiles C., 1997, ApJ 482, 193
Hellings R.W., 1986, AJ 91, 650.
Hewish A., Wolszczan A., Graham D., MNRAS 1985, 213,167
Kaspi V.M., Stinebring D.R., 1992, ApJ 392, 530
Kaspi V.M., Taylor J.H., Ryba M.F., 1994, ApJ 428, 713 [KTR94]
Kulkarni S.R., Heiles C., 1986, in Kellerman K.I., Verschuur G.L., (eds), "Galactic and Extragalactic Radio Astronomy", Springer New York, p. 95-152
Lestrade J-F., Cognard I., Biraud F., 1995, In Fruchter A., Tavani M., Backer D.C.(eds) "Millisecond pulsars : a decade of surprise", Astronomical Society of Pacific Conference Series 72, San Fransisco, 357 [LCB]
Newhall X.X.S., Standish E.M., Williams J.G., 1983, A&A 125, 150
Petit G., Boucher C., Lestrade J-F, 1989, Géod. Bull. 63, 331-341
Reynolds R.J., 1991, ApJ 372, L17
Rickett B.J., Lyne A.G., Gupta Y., 1997, MNRAS 287, 739
Romani R.W., Narayan R., Blandford R.D., 1986, MNRAS 220, 19 [RNB]
Romani R.W., Blandford R.D., Cordes J.M., 1987, Nat 328, 324
Ryba M.F., 1991, "High Precision Timing of Millisecond Pulsars", PhD Thesis, Princeton University.
Sieber W., Seiradakis J.H., 1984, AJ, 130, 257
Simonetti J.H., 1991, A&A 250, L1
Standish E.M., 1982, A&A 114, 297.
Stinebring, D.R., Smirnova, T.V., Hovis, J., et al., 1996, Proceedings of IAU Symp 160, Sydney, Austr., A.S.P. Conference Series 105, 455
Taylor J.H., Cordes J.M., 1993, ApJ 411, 674
Thorsett S.E., 1991, "Observing Millisecond and Binary Pulsars", PhD Thesis, Princeton University.
Wolszczan A., Cordes J.M., 1987, ApJ 320, L35